Megalooikonomou, K., Parolai, S., Pittore, M. (2018): Toward performance-driven seismic risk monitoring for geothermal platforms: development of ad hoc fragility curves. - *Geothermal Energy*, *6*.

DOI: http://doi.org/10.1186/s40517-018-0094-3

Megalooikonomou *et al. Geotherm Energy (2018) 6:8*
https://doi.org/10.1186/s40517-018-0094-3

Geothermal Energy

RESEARCH Open Access

Toward performance-driven seismic risk monitoring for geothermal platforms: development of ad hoc fragility curves

Konstantinos G. Megalooikonomou[1*], Stefano Parolai[2] and Massimiliano Pittore[1]

*Correspondence:
kmegal@gfz-potsdam.de
[1] GFZ German Research Centre for Geosciences, Helmholtz Centre Potsdam, Section 2.6: Seismic Hazard and Risk Dynamics, Helmholtzstraße 7, 14467 Potsdam, Brandenburg, Germany
Full list of author information is available at the end of the article

Abstract

Earthquakes, despite being a mostly natural phenomenon, may also be induced by a wide range of anthropogenic activities such as mining, fluid injection and extraction, hydraulic fracturing and geothermal reservoir processes. In recent years, the occurrence of induced and triggered seismicity and its potential impact on the built environment have heightened both public concern and regulatory scrutiny, motivating the need for an integrated risk management framework. Non-standard monitoring approaches provide valuable tools for mitigating the risk associated with earthquakes. These solutions include the use of advanced sensors and the implementation of performance-based rapid response systems for infrastructure, as well as monitoring the structural response of buildings and infrastructure in real time. Such technical solutions can be further used for validating damage forecasts determined by probabilistic approaches. The goal of this study is to establish a performance-driven monitoring system for induced seismicity. For this purpose, it is necessary to integrate analytical fragility curves in real time. These fragility curves can be derived by simplified vulnerability models that require input obtained from advanced exposure-monitoring techniques. Considering the case of induced seismicity, this also requires the expected damage to refer to non-structural components. Hence, the derived fragility curves are based on the non-structural damage criteria of typical residences. Therefore, a new approach is presented for defining analytical fragility curves of traditional or historic masonry structures, which can be found in large numbers near the geothermal platforms considered in this work.

Keywords: Non-standard monitoring, On-site monitoring system, Fragility curve, Non-structural components, Induced seismicity

Introduction

Earthquakes are mostly natural phenomena that threaten millions of people worldwide. However, they may also be induced, or triggered, by a wide range of anthropogenic activities. Some examples of those are mining, fluid injection and extraction, hydraulic fracturing (Rubinstein and Mahani 2015) and geothermal reservoir processes (Majer et al. 2007). Triggered earthquakes refer to cases where seismogenic areas already close to failure are affected by industrial activities that, despite being relatively small, can perturb this critical state enough to initiate the rupture process.

Such earthquakes may reach a relatively high magnitude and are potentially dangerous. Induced earthquakes, which are much more common, refer to events directly caused by the change in stress and strain in the Earth's crust associated with industrial activity. These events are usually characterized by small magnitudes, and therefore are mostly associated with non-structural seismic damage (Filiatrault et al. 2001) to buildings and infrastructure. However, such damage may result in non-negligible economic losses and occasionally in the partial or total disruption of activities, causing additional losses. Furthermore, the occurrence of induced seismicity is largely uncorrelated with historical seismicity, and this represents an additional uncertainty factor and further reason for concern. Indeed, in recent years, the emergence of induced seismicity and its effects on infrastructure has increased both public interest and the need for formation of new regulations for the assessment and management of induced seismicity (Bommer et al. 2015). Recent activities to control this type of seismicity by applying advanced systems were unsuccessful in most cases (Häring et al. 2008; Deichmann and Giardini 2009). Nowadays, a reasonable method to confront this risk is to apply the same tools as in the case of natural seismicity. This approach allows readiness in taking action related to the performance of anthropogenic activities known to cause earthquakes. However, the peculiar aspects of induced seismicity that emerged also in regions with no or little natural seismicity result in urgent need for amendment of the existing earthquake engineering procedures.

The ultimate goal of seismic design of a structure is to prevent structural collapse and human losses in case of an earthquake event. Over time, advances in earthquake engineering have led to a wide range of methodologies for earthquake-resistant structural design. As a result, structures built with current methods are generally able to resist expected seismic activity and preserve their structural integrity. However, although a building remains structurally sound, it can be rendered unusable due to damage to its non-structural components. Additionally, the majority of the value of some specific buildings lies in their non-structural components. For instance, it has been shown that non-structural components account for 82, 87 and 92% of building costs for offices, hotels and hospital buildings, respectively (Taghavi and Miranda 2003). Therefore, building owners may still be burdened with high expenses due to the need to repair and replace non-structural components, despite applying the current seismic design standards.

In this paper, the focus will be on the rapid and efficient modeling of an urban area from the point of view of the exposure (characterization of the number and structural features of the building stock) and of the vulnerability (considering only the possible damage to non-structural components), which are key components for the efficient and reliable implementation of risk-monitoring applications. In particular, the existing protocols for evaluating the fragility of non-structural components will be reviewed, and new fragility curves for typical building types will be proposed that have been developed for the seismic demands generally imposed upon linear and slightly non-linear models of single and multiple degrees of freedom, which is the case for the effects of induced seismicity.

Background

Exposure model

To achieve the goal of limiting the consequences of induced seismic risk in real time, the exposure and the vulnerability models for the region under consideration should be defined. Regarding exposure models, coupling remote sensing and in situ images can be optimized over broad areas for the characterization of the built environment (Pittore and Wieland 2013). This approach is feasible through the so-called remote rapid visual scanning platform (RRVS) (Fig. 1). Through this platform, several structural and non-structural building attributes are collected, following the building taxonomy proposed within the global earthquake model (GEM) (Pagani et al. 2014). The GEM taxonomy features 13 building 'attributes' that can be used to obtain an overview of the types of buildings exposed to seismic risk in a given area and to better understand their collective performance in case an earthquake strikes. The proposed taxonomy has an international scope, and it is currently being used as a basis for the GEM global exposure and consequence database (Pagani et al. 2014).

Vulnerability model

In the definition of loss, one of the most vital steps toward the estimation of the total loss in buildings due to an earthquake event is the fragility curve, which describes the relation of the response of a structure with its damage state. Specifically, a fragility curve gives the relationship between an engineering demand parameter (EDP) which can be the maximum interstory drift (IDR) or the peak floor acceleration (PFA) and the probability of exceeding a specific damage state. The main source of damage of various structural components is the structural deformation due to lateral displacements and therefore the IDR proves to be a strong index of possible damage to the structural elements of a building. While a large portion of non-structural components are sensitive to IDR, some are vulnerable primarily to PFA.

The Eurocode 8 (Cl.4.4.3.2) defines the IDR limit of a building for non-structural damage of its displacement-sensitive non-structural components for the serviceability limit state. The latter relates to structural performance for normal service conditions, under which the function of a building, its appearance, maintainability, durability and comfort for its occupants must be preserved. In that case, the IDR obtained from elastic analyses

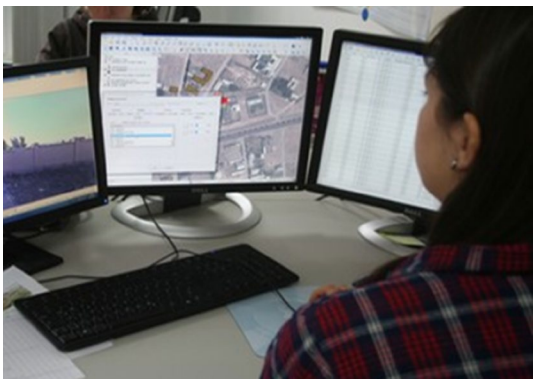

Fig. 1 Remote rapid visual scanning

should be limited to the following values, set as a function of the non-structural typology/detailing and represented by θ_{ns}, which is the limiting story drift ratio, equal to the relative interstory displacement divided by the story height.

- For buildings having non-structural components fixed in a way so as not to interfere with structural deformations: $\theta_{ns} \leq 1.0\%$.
- For buildings having ductile non-structural components: $\theta_{ns} \leq 0.75\%$.
- For buildings having non-structural components, realized with brittle materials, attached to the structure: $\theta_{ns} \leq 0.5\%$.

It is not clear from the above definitions in Eurocode 8 how ductile non-structural components are distinguished from the other mentioned types. In addition, a minimum required ductility capacity is not provided in these guidelines. Moreover, the drift limit of 1.0% for non-structural components fixed in a way not to interfere with structural deformations appears to be very high and there are not clear indications of how it is set to this value for this case. However, the above criteria provide a test bed for drift-sensitive non-structural damage to be considered as damage thresholds in the analytical definition of fragility curves.

According to D'Ayala and Meslem (2013), analytical fragility assessment procedures are usually based on the ground motion intensity-to-structural response functions and on the structural response-to-damage state functions. The latter is the product of structural and damage analysis and a certain level of uncertainty should be accounted for when performing seismic risk assessment. To take into account these uncertainties, firstly, it is necessary to identify the sources of uncertainty related to capacity demand and damage threshold definitions and secondly to quantify and model these uncertainties when constructing analytical fragility curves. With regard to the structural analysis stage, capacity and demand-related uncertainties are commonly accounted for in the estimation of buildings' performance (Maio and Tsionis 2015). Non-structural components, such as masonry infill walls in reinforced concrete (RC) buildings, may contribute to the seismic behavior of the structure or can be accounted for in loss estimation, since as it is already mentioned they represent a significant proportion of building's construction cost. In structural assessment methodologies, there are different choices available for the mathematical modeling and the type of analysis to be performed. The uncertainties defined in these models depend on the complexity level to be considered in the fragility assessment. The equivalent single-degree-of-freedom system (ESDOF) is widely used in a number of simplified procedures when defining the performance and damage state of structures for analytical computation of fragility curves.

Methods

To promptly forecast the expected damage (performance), suitable fragility curves determined by probabilistic approaches are necessary. Based on the performance level, a customized rapid damage forecasting system (Parolai et al. 2015, 2017; Bindi et al. 2016) (Fig. 2) may then be developed. Such system would issue an alert according to pre-defined thresholds on the incoming ground motion and considering the expected performance of one or more specific structures.

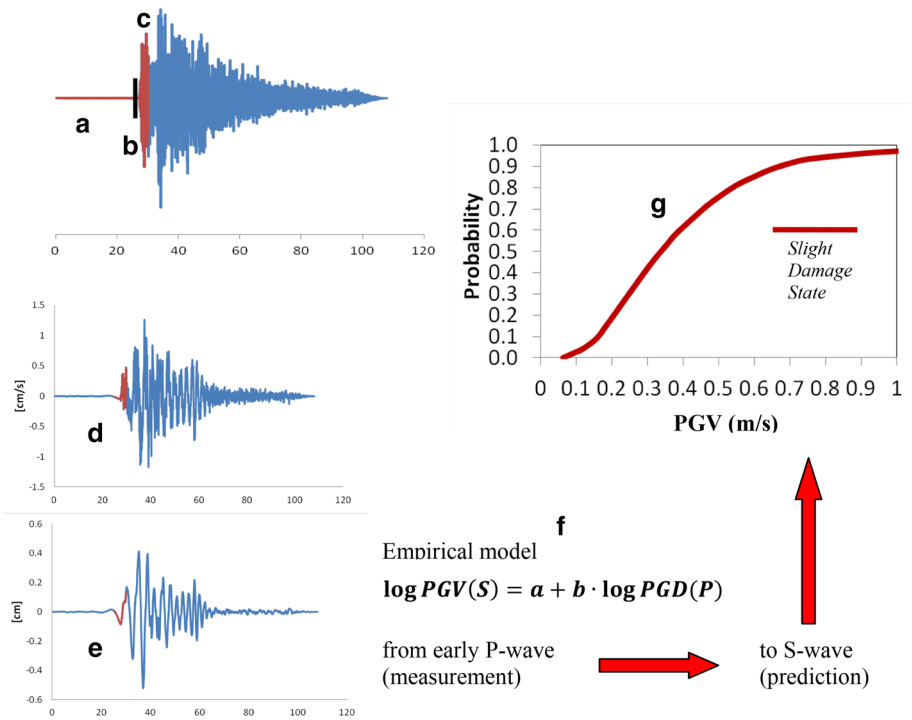

Fig. 2 The developed rapid damage forecasting system (Bindi et al. 2016) **a** Real-time strong motion acquisition; **b**, **c** as soon as the P-wave onset is triggered, strong motion parameters are estimated over a 3 s time window; **d** estimation of parameters over velocity integrated signal; **e** estimation of parameters over displacement integrated signal; **f** prediction of PGV for S-waves using the peak ground displacement (PGD) over P-waves and using semi-empirical relations (Zollo et al. 2010); **g** the fragility curves of the building are used to compute the probabilities of exceeding damage states

In the considered test site, the analysis of the collected exposure information indicates that traditional or historical masonry structures occur in large numbers near the mostly rural areas close to the geothermal platforms in Alsace region in France (Fig. 3). Two general classes of structures, namely unreinforced masonry (URM) and timber frame masonry (TFM) buildings, have been considered, and simple performance assessment models (Vamvatsikos and Pantazopoulou 2015; Kouris and Kappos 2014) have been adopted to carry out a preliminary vulnerability assessment for these classes of structures. The objective is to rapidly identify buildings and their non-structural components that are at greater risk in the event of an induced earthquake and to model their non-structural fragility.

Unreinforced masonry buildings (URM)

While steel or concrete frames are mostly lumped systems with stiff diaphragms, URM buildings have distributed mass and stiffness commonly in combination with flexible diaphragms. This fact obstructs the adoption of the established methodologies to URM buildings. Specifically, the fundamental mode shape of the latter buildings involves a low percentage of the total mass of the building below the 75% limit required for the good performance of ESDOF-based methods. To solve this issue, the simplified procedure of Vamvatsikos and Pantazopoulou (2015) was adopted. In their procedure, the dynamic

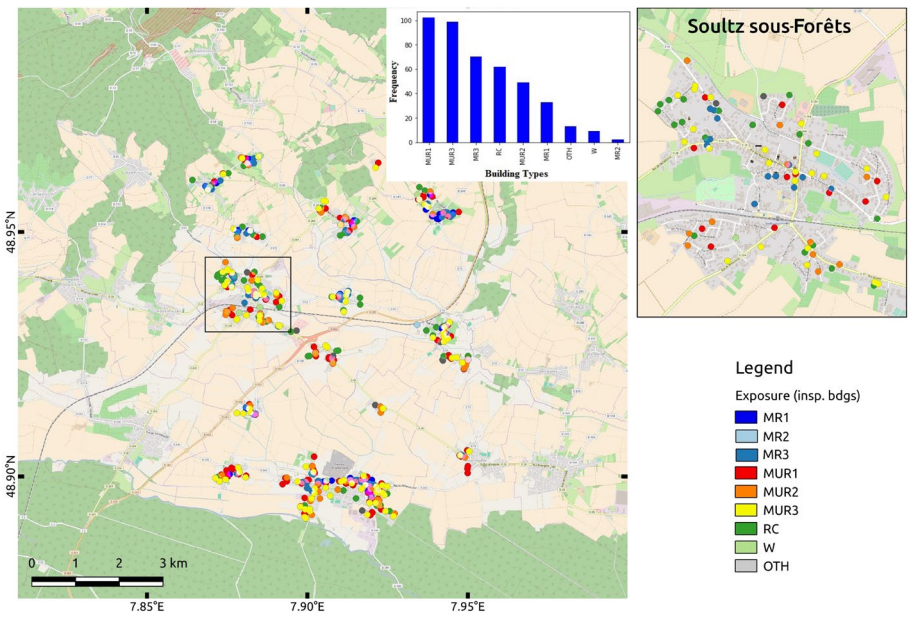

Fig. 3 Exposure model including 500 buildings' assessment with remote rapid visual scanning in the Alsace region in France (MUR = unreinforced masonry, MR = reinforced masonry, RC = reinforced concrete, W = wood, OTH = other, 1 = one-story building, 2 = two-story building with rigid diaphragm, 3 = two-story building with flexible diaphragm)

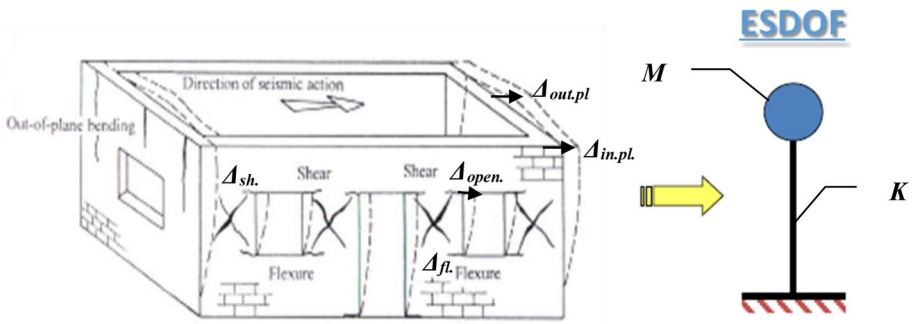

Fig. 4 Equivalent single-degree-of-freedom (ESDOF) representation of typical box-shape unreinforced masonry (URM) building under earthquake-induced loading taking into account typical deformation components in the fundamental mode shape [Δ_{sh}: horizontal displacement due to shear deformation, Δ_{fl}: horizonal displacement due to flexural deformation, Δ_{open}: horizontal displacement contribution of masonry wall openings, $\Delta_{in,pl}$: in-plane horizontal masonry wall displacement (consists of Δ_{sh}, Δ_{fl}, Δ_{open}), $\Delta_{out,pl}$: out-of-plane horizontal masonry wall displacement due to out-of-plane bending, *M*: ESDOF generalized mass, *K*: ESDOF generalized stiffness]

URM building response is represented. Global response indices are transformed to local deformation measures in closed-form seismic assessment solution, both for demand and supply in the critical structural locations. The solution involves the definition of the fundamental vibration mode, approximated by 3D shape function, consistent with the building's boundary conditions. Strength and deformation indices are adopted for the evaluation of the acceptance criteria. Typical local failures are estimated through a local shape of deformation, while the model captures the global dynamic characteristics (Fig. 4). The adopted method allows the automation of the necessary calculations

through closed-form expressions. The latter involve as input only key geometric characteristics of the box-shape masonry building (Tomazevic 2006, Fig. 4) as well as the wall thickness, shear strength and shear modulus of the URM wall, all of which can be easily determined. On the other hand, the applicability of the described simplified ESDOF procedure is restricted to simple box-shape URM buildings with rectangular floor plans and flexible or rigid floor diaphragms and therefore its use for seismic assessment of irregular URM buildings is not recommended.

Timber-framed masonry buildings (TFM)

TFM walls are reinforced with timber elements, both horizontal and vertical but also X-type diagonal braces. It is evident, historically, since the Bronze Age that the timber reinforcement into masonry walls is strongly related to seismic resistance in earthquake-prone areas. In TFM walls there is also recent experimental and numerical evidence (Kouris and Kappos 2014) that the contribution of the diagonal braces is vital for walls' lateral behavior in the non-linear range due to early detachment of the masonry infill from the surrounding timber frame in the event of an earthquake. In addition, it is observed that for very low horizontal displacement, the diagonals in tension detach from the surrounding frame. Therefore, it is suggested (Kouris and Kappos 2014) that the diagonals should contribute to the lateral behavior only in compression and moreover the infill masonry walls of the timber frame should not be considered in the analytical model. Based on these considerations, a macro-model was proposed (Kouris and Kappos 2012, 2014, Fig. 5), where its input can be easily determined since it involves only the key geometric characteristics of the timber panels and the timber strength. The latter model facilitates the seismic assessment of TFM walls resulting in a valuable tool for simplified seismic vulnerability and risk analyses (Kouris and Kappos 2015). Based on the resulting pushover curves produced by pushover analysis (Antoniou and Pinho 2004) of the TFM walls' macro-model, a shape function is defined for the derivation of the ESDOF properties which is similar to the methodology already described for URM buildings (Vamvatsikos and Pantazopoulou 2015). In this way, the corresponding fragility curves are derived in terms of peak ground acceleration (PGA) with the aid of structural analysis for a gradually increasing intensity (incremental dynamic analysis—IDA, Vamvatsikos and Cornell 2002). The correlation of the PGA values of the recordings used in the IDA analysis with the corresponding PGV values follows the rule that for very flexible structures (very high fundamental periods), the relative velocity response spectrum of the used record tends to the peak ground velocity (PGV).

Results and discussion

Induced ground motion database

The Web-based Pacific Earthquake Engineering Research Center (PEER) ground motion database (PEER-NGA-East Database 2017) provides tools for searching, selecting and downloading ground motion data. To apply an incremental time history dynamic analysis (IDA) (Vamvatsikos and Cornell 2002) to the ESDOF models of the masonry buildings under consideration in this study, there is a need for realistic induced ground motion records.

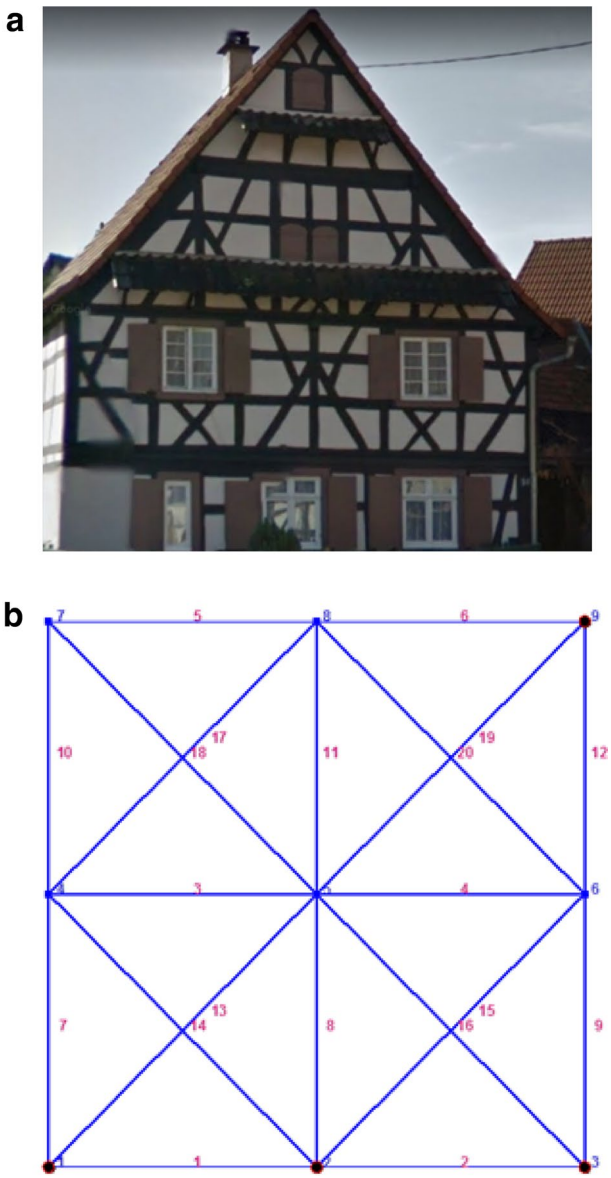

Fig. 5 **a** Example of a timber-framed masonry building (TFM). **b** TFM wall model with panels incorporating X-type diagonal braces

The PEER ground motion database was therefore examined to identify records of induced ground motion, of which 20 were selected. In the entire database, nine induced earthquake events are recorded, mainly located in the states of Oklahoma, Arkansas and Texas in the USA (Table 1). These earthquake events were shallow, with depths ranging from 3 to 14 km. Of the available stations recording these events, a selection was made of the records that were closer to the epicenter, with epicentral distances ranging between 5 (the closest available station to these events) and 55 km. The moment magnitude scale range of the selected events was between 3 and 5.5 (Fig. 6). The range of peak ground acceleration (PGA) values can also be seen in Fig. 6.

Table 1 Earthquake events involving induced seismicity identified in the PEER database

EQ-ID	EQ-ID database	Year	Name	Location	M_w	Epicenter latitude (deg)	Epicenter longitude (deg)	Depth (km)
1	57	2010	Lincoln_2010-02-27	Lincoln OK	4.18	35.553	− 96.752	4
2	66	2010	Slaughterville_2010-10-13	Slaughterville OK	4.36	35.202	− 97.309	14
3	67	2010	Guy_2010-10-15	Guy AR	3.86	35.276	− 92.322	5
4	73	2010	Arcadia_2010-11-24	Arcadia OK	3.96	35.627	− 97.246	3
5	74	2010	BethelAcres_2010-12-12	Bethel Acres OK	3.23	35.392	− 96.995	4
6	76	2010	Guy_2010-11-20	Guy AR	3.90	35.316	− 92.317	5
7	80	2011	Greenbrier_2011-02-28	Greenbrier AR	4.68	35.265	− 92.34	4
8	91	2011	Sparks_2011-11-06	Sparks OK	5.68	35.537	− 96.747	9
9	92	2011	Comal_2011-10-20	Comal TX	4.71	28.81	− 98.15	4

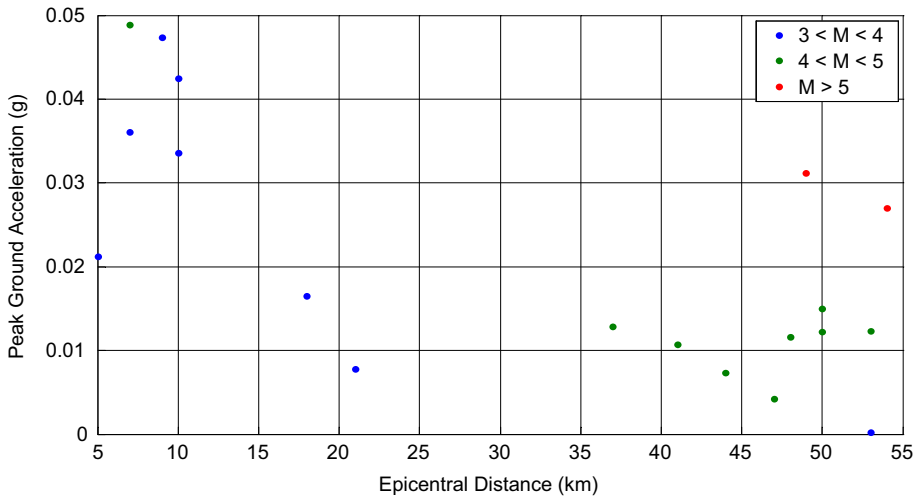

Fig. 6 Peak ground acceleration (PGA) of the ground motions selected from the PEER seismicity database as a function of epicentral distance (the data are based on the availability of seismic stations in PEER database that recorded each event in the range of epicentral distance considered in this study)

In Figs. 7, 8 and 9, the elastic response spectra for some of the ground motion records under consideration in this study are presented. A comparison is also made with the type 2 elastic response spectrum of Eurocode 8 (CEN 2004) for earthquake magnitudes up to 5.5. It can be seen that low-rise structures—having mainly low fundamental period (that occur in large numbers near the geothermal platforms in remote and less populated areas)—are mostly affected by this type of ground motion—undergoing higher spectral acceleration (attributed to the high-frequency content of the induced seismic waves from shallow earthquakes, having short duration and causing near-field damage). The maximum spectral acceleration in some cases (Figs. 7, 8) is comparable with that of Eurocode 8 elastic response spectrum for very soft soils (soil types according to Eurocode 8 C, D and E).

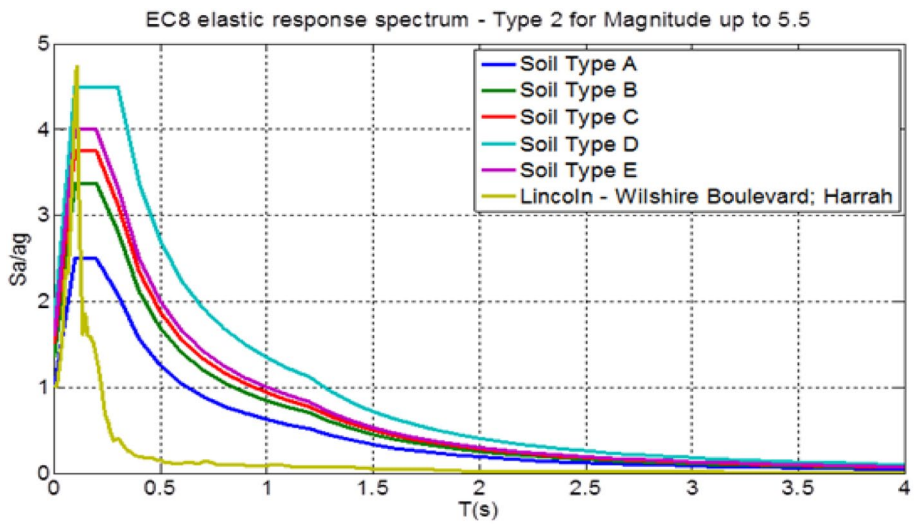

Fig. 7 Elastic response spectra of the induced seismic ground motions obtained from the PEER database and their comparison with the Eurocode 8 type 2 elastic response spectrum for magnitudes up to 5.5. In the legend, the soil types A–E (rock [A] to softer soils [E]) refer to the different Eurocode 8 type 2 elastic response spectra produced for different soil conditions according to Eurocode 8. The remaining term in the legend refers to the name of the seismic station (PEER database) which recorded the induced seismic event's (Lincoln, Table 1) ground motion used to produce the elastic response spectrum

Unreinforced masonry buildings (URM)

The application of the methodology presented in this work to produce the analytical fragility curves for URM buildings is demonstrated here on a simple unreinforced masonry model structure which was tested under simulated ground motions on a shake table by Bothara et al. (2010). The experimental fragility curve based on the experimental damage (measured drifts from incremental levels of shaking) is provided for comparison with those obtained by the analytical procedures. The building model was built at a scale of 1:2. The model had 0.11 m thick masonry walls, a rectangular floor plan of 2.88 m × 1.92 m and was a two-story structure with a first floor height of 1.34 m, a second floor height of 1.14 m and a roof gable rising by 0.815 m. The structure was first tested using a suite of ground motions in the longitudinal direction, scaling them to PGA values in the range of 0.2–0.8*g*. This testing was repeated by shaking the structure in the short direction of its plan. Due to the lack of stiff floor panels and connections, no diaphragm action was assumed.

Figure 10 provides the analytical fragility curves for the pre-yielding damage state (which is the case for induced seismicity demands) with 0.1% drift limit. The curve was produced using IDA of the ESDOF of the above-mentioned scaled URM building, employing the induced ground motions obtained from the PEER database previously presented and applied in the longitudinal and transverse building plan directions. It can be seen that the fragility curve produced by the elastic time history analysis in the transverse (weak) direction of the URM building is close to the experimental fragility curve obtained from the experimental data. In addition, the drift limit for damage to drift-sensitive brittle non-structural components provided by Eurocode 8 was also applied to the results of the IDA in the short building plan direction and the corresponding fragility curve also provided. It is noteworthy that the roof tiles

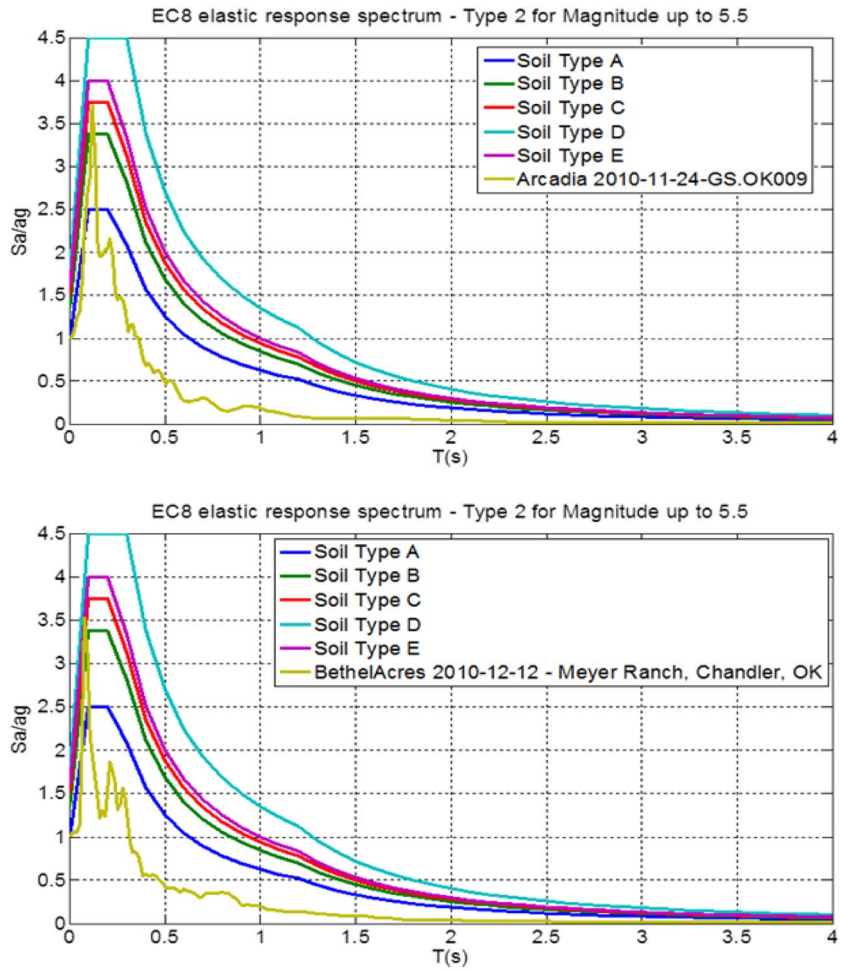

Fig. 8 Elastic response spectra of the induced seismic ground motions obtained from the PEER database and their comparison with the Eurocode 8 type 2 elastic response spectrum for magnitudes up to 5.5. In the legend, the soil types A–E (rock [A] to softer soils [E]) refer to the different Eurocode 8 type 2 elastic response spectra produced for different soil conditions according to Eurocode 8. The remaining term in the legend refers to the name of the seismic station (PEER database) which recorded the induced seismic event's (Arcadia, BethelAcre, Table 1) ground motion used to produce the elastic response spectrum

(drift-sensitive brittle non-structural components) of the experimental model that were not connected to the roof structure scattered badly during the experiment and a few of them slid off the roof when subjected to a PGA of 0.5*g*. However, in real event, such tiles would slide off at much lower level of shaking as it is observed in PEER earthquake reconnaissance reports (PEER-Earthquake Reconnaissance Reports 2017). By applying the Eurocode 8 drift limit to this case, the corresponding fragility curve could not capture the PGA corresponding to the experimental failure of the roof tiles. The correct drift limit in this case for drift-sensitive brittle non-structural components should therefore be 0.1% or lower.

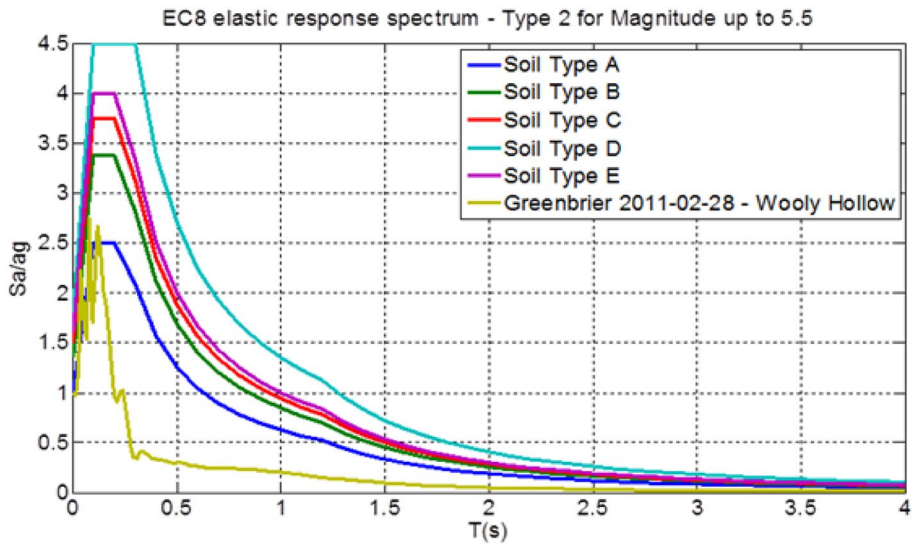

Fig. 9 Elastic response spectra of the induced seismic ground motions obtained from the PEER database and their comparison with the Eurocode 8 type 2 elastic response spectrum for magnitudes up to 5.5. In the legend, the soil types A–E (rock [A] to softer soils [E]) refer to the different Eurocode 8 type 2 elastic response spectra produced for different soil conditions according to Eurocode 8. The remaining term in the legend refers to the name of the seismic station (PEER Database) which recorded the induced seismic event's (Greenbrier, Table 1) ground motion used to produce the elastic response spectrum

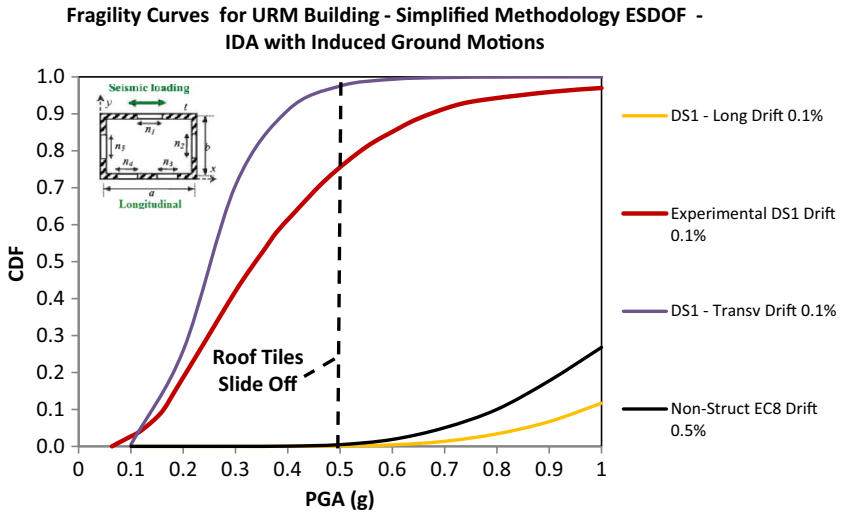

Fig. 10 Analytical fragility curves for first damage state (pre-yielding damage state—DS1) for an unreinforced masonry building (URM) tested experimentally on a shake table. Longitudinal (Long) and transversal (Transv) or short plan view directions of shaking are considered. The Eurocode 8 (EC8) drift limit for brittle non-structural components is also applied. The vertical dashed line dictates the experimental PGA threshold over which detachment of the roof tiles of the URM building under study has been observed

Timber-framed masonry buildings (TFM)

In the case of TFM buildings, to the authors' best knowledge, there is only experimental evidence from the cyclic excitation of TFM walls and not shake table tests of a TFM building model. Therefore, the analytical procedure adopted here for the

definition of the fragility curves of TFM buildings is validated through the non-linear static analysis of TFM walls. Based on the analytical model, a shape function of the box-shaped TFM building is defined to derive the ESDOF properties for the corresponding fragility curves to be obtained in terms of PGA with the aid of IDA.

The macro-model adopted by Kouris and Kappos (2014) involves the discretization of the building into individual timber-framed panels with equivalent truss model with elastic horizontal and vertical truss elements, but non-linear diagonal truss elements (Fig. 5b). The adopted empirical model is then used for defining the non-linear material constitutive law of non-linear truss elements representing the diagonal braces that contribute only in compression (Fig. 11). An example of the resulting pushover curve (Antoniou and Pinho 2004) is given in Fig. 12, where the analytical capacity curve is compared with the experimental results by Meireles et al. (2012). It can be seen that there is good agreement between the numerical and experimental results. Therefore, the empirical model of Kouris and Kappos (2014) is advisable for the definition of the analytical fragility curves through IDA. For the induced seismicity demands, only the pre-yielding damage state is of interest.

Proposed building-specific analytical fragility curves for URM and TFM buildings

Considering some real TFM and URM building cases in Alsace France (Fig. 3), the corresponding fragility curves are derived in terms of peak ground acceleration (PGA) with the aid of structural analysis for a gradually increasing intensity (incremental dynamic analysis—IDA). The latter analysis of ESDOF of the building cases under study was performed with the MATLAB (Mathworks 2017) toolbox FEDEAS Lab (Filippou and Constantinides 2004). The correlation of the PGA values of the recordings used in the IDA analysis with the corresponding PGV values follows the rule as already mentioned, and that for very flexible structures (very high fundamental periods) the relative velocity response spectrum of the used record tends to the peak ground velocity (PGV). The induced ground motions obtained from the PEER database previously presented were employed and applied in the transverse/short/weak building plan direction. The fundamental periods of these structures were verified with ambient noise vibration measurements using sensors (Boxberger et al. 2017) located on each floor of the buildings

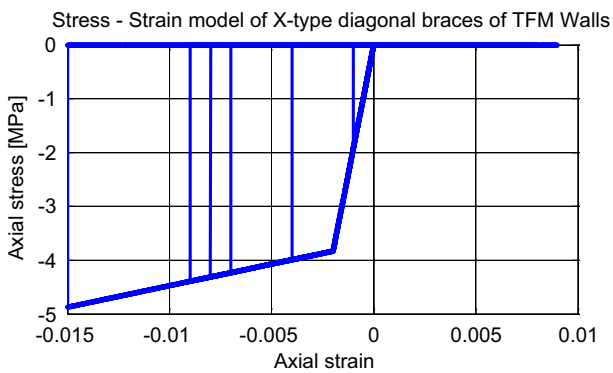

Fig. 11 Stress–strain material model of the non-linear truss elements representing X-type timber diagonal braces

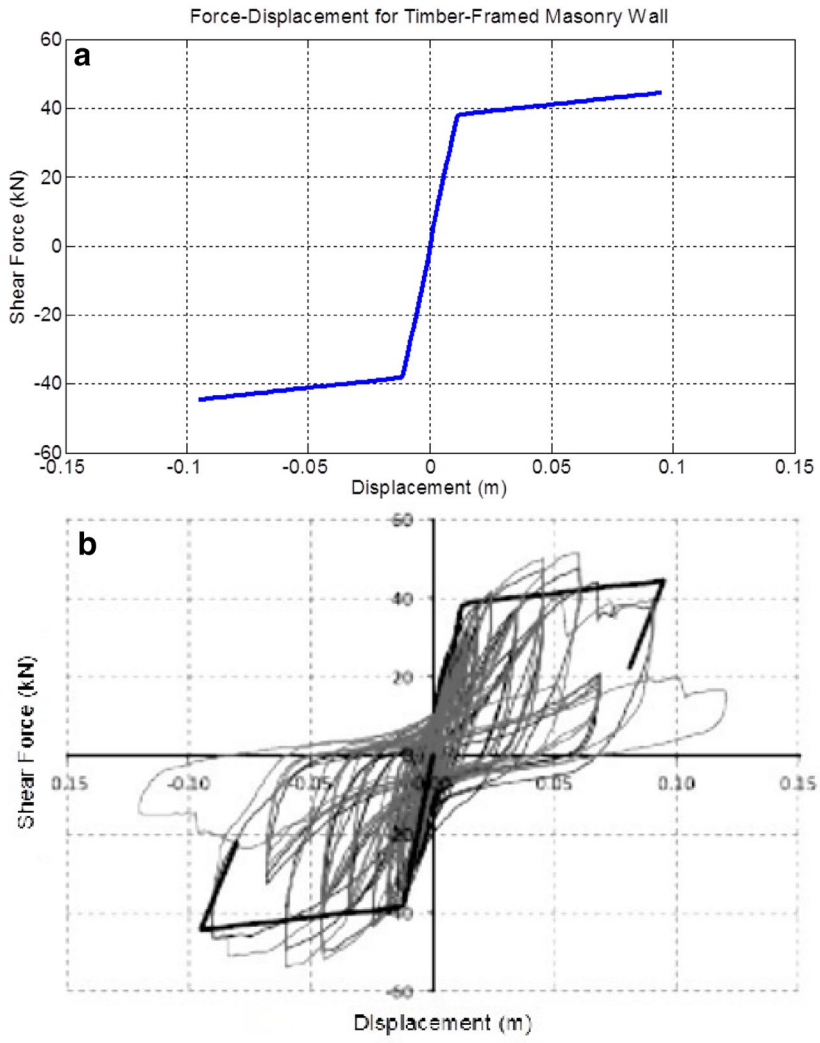

Fig. 12 Comparison of the pushover curves from the methodology adopted by Kouris and Kappos (2014) **a** and the experimental results by Meireles et al. (2012) **b**

Table 2 Real URM and TFM buildings located near the geothermal platforms in Alsace region in France

No.	Building type	Building latitude	Building longitude	Fundamental ESDOF model period (s)	Fundamental frequency sensor (Hz)
1	URM	48.964946	7.881095	0.17	5.5
2	URM	48.902075	7.874917	0.37	2.7
3	URM	48.905270	7.950266	0.11	9
4	TFM	48.914307	7.882233	0.15	6.7
5	URM	48.932865	7.874377	0.32	3.1

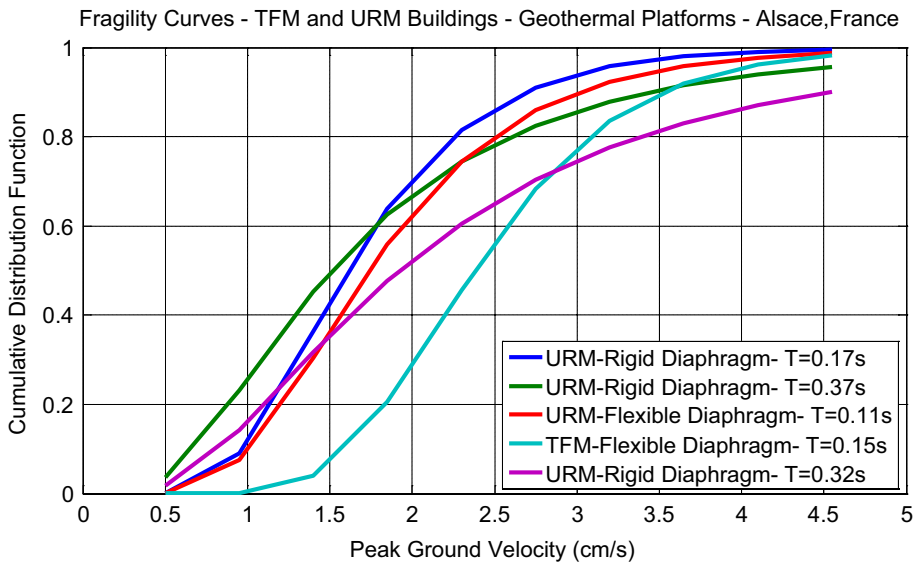

Fig. 13 Proposed analytical fragility curves for first damage state (pre-yielding damage state—DS1—0.1% drift limit for non-structural damage) for unreinforced masonry buildings (URM) and timber-framed masonry buildings (TFM). The buildings are located near the geothermal platforms in Alsace France and are loaded in the weak/short plan view direction of shaking. The fundamental period of these structures was verified with ambient noise measurements through applied sensors (Boxberger et al. 2017)

under study (Table 2). Moreover, the main geometry required as input for the simplified vulnerability models was taken through field inspection of these buildings. The results are shown in Fig. 13. It can be seen that the fragilities for URM buildings have more or less the same range of probability of damage, while the more earthquake-resistant TFM building is less fragile for low and medium intensities. Finally, it should be noted that a permanent sensor (Boxberger et al. 2017) that is running the rapid damage forecasting system presented in Fig. 2 is installed in the townhall of Keffenach (URM building No. 1 in Table 2) in Alsace region in France near the geothermal platforms of this region (Soultz-sous-Forêts and Rittershoffen). In this sensor, the fragility curve for this URM building (fundamental period $T = 0.17$ s)—depicted in Fig. 13—is incorporated.

Conclusions

A prompt and reliable performance-based monitoring may be an effective solution to improve the management of risk arising from induced and triggered seismicity. Considering the expected magnitude and characteristics of such earthquake events, it was decided to focus on non-structural components, which often represent the majority of the cost of a building. To provide a rapid forecasting of the expected resulting loss, a set of fragility curves describing the damage to non-structural components have been estimated. In the proposed conceptual approach, several innovative methodologies are used based on the key geometric characteristics that are collected and represented in the exposure model. The adopted procedure can be used to assess the seismic behavior of masonry buildings and it is deemed to be a useful tool for seismic vulnerability and risk analyses. A shape function is defined for the derivation of the ESDOF properties of URM and TFM buildings. In this way, the corresponding fragility curves are

derived in terms of peak ground acceleration (PGA) with the aid of structural analysis for a gradually increasing intensity (incremental dynamic analysis—IDA). This simplified model reproduces the global vibration characteristics, while also employing a local deformation shape to allow the estimation of typical local failures. An advantage of the procedure is that it allows the automation of the necessary calculations to reliably extend the seismic vulnerability analysis to large inventories of buildings. Finally, the real-time performance-based on-site rapid response system for induced seismicity was introduced, incorporating these analytical fragility curves for non-structural components of masonry buildings. These curves have been developed for linear and slightly non-linear systems of single and multiple degrees of freedom for the range of intensities expected for induced seismicity. Based on the above described exposure and vulnerability model, a custom-tailored real-time risk-monitoring system has been developed which issues an alert if the likelihood of observing (non-structural) damage in a specific building and its neighborhood exceeds a given threshold. This will prove useful for both local end users and industrial stakeholders, with a clear perspective for a better understanding of the risk related to induced and triggered seismicity and its sound management.

Abbreviations

RRVS: remote rapid visual scanning platform; GEM: global earthquake model; EDP: engineering demand parameter; IDR: maximum Interstory drift; PFA: peak floor acceleration; RC: reinforced concrete; W: wood; ESDOF: equivalent single-degree-of-freedom system; URM or MUR: unreinforced masonry; MR: reinforced masonry; OTH: other; TFM: timber frame masonry; IDA: incremental dynamic analysis; PGA: peak ground acceleration; PGV: peak ground velocity; PEER: Pacific Earthquake Engineering Research Center; CDF: cumulative distribution function; EC8: Eurocode 8; DS1: pre-yielding damage state.

Authors' contributions

KGM did the data analysis, comparison and interpretation. SP contributed to the performance-based monitoring system proposal. MP gave guidance and supported the exposure model. All authors read and approved the final manuscript.

Author details

[1] GFZ German Research Centre for Geosciences, Helmholtz Centre Potsdam, Section 2.6: Seismic Hazard and Risk Dynamics, Helmholtzstraße 7, 14467 Potsdam, Brandenburg, Germany. [2] National Institute of Oceanography and Experimental Geophysics (OGS), Borgo Grotta Gigante 42/C, 34010 Trieste, Sgonico, Italy.

Acknowledgements

The authors would like to thank Kevin Fleming for his comprehensive check of the English language and the anonymous reviewers for their contributions and manuscript improvement.

Stefano Parolai—previously at GFZ.

Competing interests

The authors declare that they have no competing interests.

Ethics approval and consent to participate

Not applicable.

Funding

This work has been supported financially by the European Union funded project DESTRESS (http://www.destress-h2020.eu) (Work Package 3.4), (Grant No. 691728).

Publisher's Note

Received: 26 February 2018 Accepted: 4 June 2018
Published online: 11 June 2018

References

Antoniou S, Pinho R. Development and verification of a displacement-based adaptive pushover procedure. J Earthquake Eng. 2004;8(5):643–61. https://doi.org/10.1080/13632460409350504.

Bindi D, Iervolino I, Parolai S. On-site structure-specific real-time risk assessment: perspectives from the REAKT project. Bull Earthq Eng. 2016;14(9):2471–93. https://doi.org/10.1007/s10518-016-9889-4.
Bommer JJ, Crowley H, Pinho R. A risk-mitigation approach to the management of induced seismicity. J Seismol. 2015;19:623–46. https://doi.org/10.1007/s10950-015-9478-z.
Bothara JK, Dhakal RP, Mander JB. Seismic performance of an unreinforced masonry building: an experimental Investigation. Earthq Eng Struct Dynam. 2010;39:45–68. https://doi.org/10.1002/eqe.932.
Boxberger T, Fleming K, Pittore M, Parolai S, Pilz M, Mikulla S. The multi-parameter wireless sensing system (MPwise): its description and application to earthquake risk mitigation. Sensors. 2017;17(10):2400. https://doi.org/10.3390/s17102400.
CEN. *Eurocode 8*: design of structures for earthquake resistance—part I: general rules, seismic actions and rules for buildings. Brussels: European Committee for Standardization (CEN); 2004.
D'Ayala D, Meslem A. Sensitivity of analytical fragility functions to capacity-related parameters. Pavia: GEM Technical Report 2013-X; 2013.
Deichmann N, Giardini D. Earthquakes induced by the stimulation of an enhanced geothermal system below Basel (Switzerland). Seismol Res Lett. 2009;80(5):784–98. https://doi.org/10.1785/gssrl.80.5.784.
Filiatrault A, Christopoulos C, Stearns C. Guidelines, specifications and seismic performance characterization of nonstructural building components and equipments, PEER Report 2002/05. Berkeley: University of California; 2001.
Filippou FC, Constantinides M. FEDEAS Lab—Getting Started Guide and Simulation Examples, NEESgrid Report 2004-22 and SEMM Report 2004-05. 2004.
Häring MO, Schanz U, Ladner F, Dyer BC. Characterisation of the Basel 1 enhanced geothermal system. Geotherm J. 2008;37:469–95. https://doi.org/10.1016/j.geothermics.2008.06.002.
Kouris LAS, Kappos AJ. Detailed and simplified non-linear models for timber-framed masonry structures. J Cult Heritage. 2012;13(1):47–58. https://doi.org/10.1016/j.culher.2011.05.009.
Kouris LAS, Kappos AJ. A practice—oriented model for pushover analysis of a class of timber-framed masonry buildings. Eng Struct J. 2014;75:489–506. https://doi.org/10.1016/j.engstruct.2014.06.012.
Kouris LAS, Kappos AJ. Fragility curves and loss estimation for traditional timber-framed masonry buildings in Lefkas, Greece. In: Psycharis I, Pantazopoulou S, Papadrakakis M, editors. Seismic assessment, behavior and retrofit of heritage buildings and monuments, vol. 37. Cham: Springer; 2015. https://doi.org/10.1007/978-3-319-16130-3_8.
Maio R, Tsionis G. Seismic fragility curves for the European building stock. Brussels: JRC Technical Report, European Commission; 2015.
Majer EL, Baria R, Stark M, Oates S, Bommer J, Smith B, Asanuma H. Induced seismicity associated with enhanced geothermal systems. Geotherm J. 2007;36(3):185–222. https://doi.org/10.1016/j.geothermics.2007.03.003.
Mathworks. MATLAB: User's Guide (r2017a). 2017.
Meireles H, Bento R, Cattari S, Lagomarsino S. A hysteretic model for "frontal" walls in Pombalino buildings. Bull: Earthq Eng; 2012. https://doi.org/10.1007/s10518-012-9360-0.
Pagani M, Monelli D, Weatherill G, Danciu L, Crowley H, Silva V, Henshaw P, Butler L, Nastasi M, Panzeri L, Simionato M, Vigano D. OpenQuake engine: an open hazard (and risk) software for the global earthquake model. Seismol Res Lett. 2014;85(3):692–702. https://doi.org/10.1785/0220130087.
Parolai S, Bindi D, Boxberger T, Milkereit C, Fleming K, Pittore M. On-site early warning and rapid damage forecasting using single stations: outcomes from the REAKT project. Seismol Res Lett. 2015;86(5):12. https://doi.org/10.1785/0220140205.
Parolai S, Oth A, Boxberger T. Performance of the GFZ decentralized on-site earthquake early warning software (GFZ-Sentry): application to K-NET and KiK-Net recordings, Japan. Seismol Res Lett. 2017;88(6):1480–90. https://doi.org/10.1785/0220170048.
PEER-Earthquake Reconnaissance Reports. Pacific Earthquake Engineering Research Center, University of California, Berkeley; 2017. http://peer.berkeley.edu/publications/earthquake_recon_reports.html. Accessed 15 Feb 2017.
PEER-NGA-East Database. Pacific Earthquake Engineering Research Center, University of California, Berkeley; 2017. http://peer.berkeley.edu/ngaeast/. Accessed 1 Feb 2017.
Pittore M, Wieland M. Toward a rapid probabilistic seismic vulnerability assessment using satellite and ground-based remote sensing. Nat Hazards. 2013;68(1):115–45. https://doi.org/10.1007/s11069-012-0475-z.
Rubinstein JL, Mahani AB. Myths and facts on wastewater injection, hydraulic fracturing, enhanced oil recovery, and induced seismicity. Seismol Res Lett. 2015;86(4):1060–7. https://doi.org/10.1785/0220150067.
Taghavi S, Miranda E. Response assessment of nonstructural building elements, PEER report 2003/05. Berkeley: University of California; 2003.
Tomazevic M. Series on innovation in structures and construction. Earthquake-resistant design of masonry buildings, vol. 1. London: College Press; 2006.
Vamvatsikos D, Cornell CA. Incremental dynamic analysis. Earthq Eng Struct Dynam. 2002;31(3):491–514. https://doi.org/10.1002/eqe.141.
Vamvatsikos D, Pantazopoulou SJ. Development of a simplified mechanical model to estimate the seismic vulnerability of heritage unreinforced masonry buildings. J Earthq Eng. 2015;20(2):298–325. https://doi.org/10.1080/13632469.2015.1060583.
Zollo A, Amoroso O, Lancieri M, Wu Y-M, Kanamori H. A threshold-based earthquake early warning using dense accelerometer networks. Geophys J Int. 2010;183:963–74. https://doi.org/10.1111/j.1365-246x.2010.04765.x.